Ionic Liquids-infused Slippery Surface for Temperature stability, Shear Resistance and Corrosion Resistance

Yi Chen,[ac] Zhiguang Guo*[ab]

[a] State Key Laboratory of Solid Lubrication, Lanzhou Institute of Chemical Physics, Chinese Academy of Sciences, Lanzhou 730000, People's Republic of China. *E-mail: zguo@licp.cas.cn; Fax: +86-931-8277088; Tel: +86-931-4968105*

[b] Hubei Collaborative Innovation Centre for Advanced Organic Chemical Materials and Ministry of Education Key Laboratory for the Green Preparation and Application of Functional Materials, Hubei University, Wuhan 430062, People's Republic of China

[c] University of Chinese Academy of Sciences, Beijing 100049, People's Republic of China

1 Physical performance analysis of ILs

To realize better thermal stability, the ILs of $[VC_nIM][NTf_2]$ (n=4,6,8) with different length of carbon chains were selected as the lubricant, and the thermal stability of different length of carbon chain of ILs with anion of $[NTf_2]$ and the PFPE were investigated by TG (Fig.S1 a-c and Table S1). As the Fig. S1a exhibits, the initial decomposition temperatures (T_d) are about 390 ℃ and 210 ℃ for the ILs and the PFPE, respectively. The T_d of ILs are all higher than the PFPE, which shows a wider range of applied temperatures of ILs'. Besides, the temperature when the residual mass reached 10% of initial mass ($T_{10\%}$) was also used to analysis the thermal stability. Especially, the $[VHIM][NTf_2]$ is more stable at high temperature conditions. To further explore the lowest temperature of the ILs, the glass transition temperature (T_g) was tested by DSC (Fig.S1 d), which were all about -70 ℃. The changes of specific heat capacity in the temperature-rise process of $[VBIM][NTf_2]$, $[VHIM][NTf_2]$ and $[VOIM][NTf_2]$ are 0.321 J/($g*k$), 0.2841 J/($g*k$) and 0.321 J/($g*k$), respectively. According to the definition equation of specific heat capacity $Q = c*m*\Delta T$, (where Q, c, m and ΔT are quantity of heat, specific heat capacity, mass and changes of temperature, respectively), at the same conditions, the ILs with high specific heat capacity needs more heat to maintain balance. This means that the ILs with low specific heat capacity are more thermal stable. Thus, the $[VHIM][NTf_2]$ with low specific heat capacity is needed in this work. For the miscibility tests, 0.5 ml $[VHIM][NTf_2]$ was added in 0.5ml water dyed by MB and 0.5 ml ethanol dyed by RhB. The inset image in Fig. S1b show the miscibility state of $[VHIM][NTf_2]$ with water (left) and ethanol (right) after ultrasound treating 10 min and keeping standing 5 min to reach a stable state. There was distinct layering in the left image, but become a whole in the right image, which indicated that the $[VHIM][NTf_2]$ was immiscible with water but was miscible well with ethanol. At the beginning, the dyed water was on the top, and $[VHIM][NTf_2]$ was on the bottom. But the stable state (the left of inset image in Fig. S1. (b)) show that the dye was absorbed by the $[VHIM][NTf_2]$ mostly. Thus, the bottom shows the color of MB.
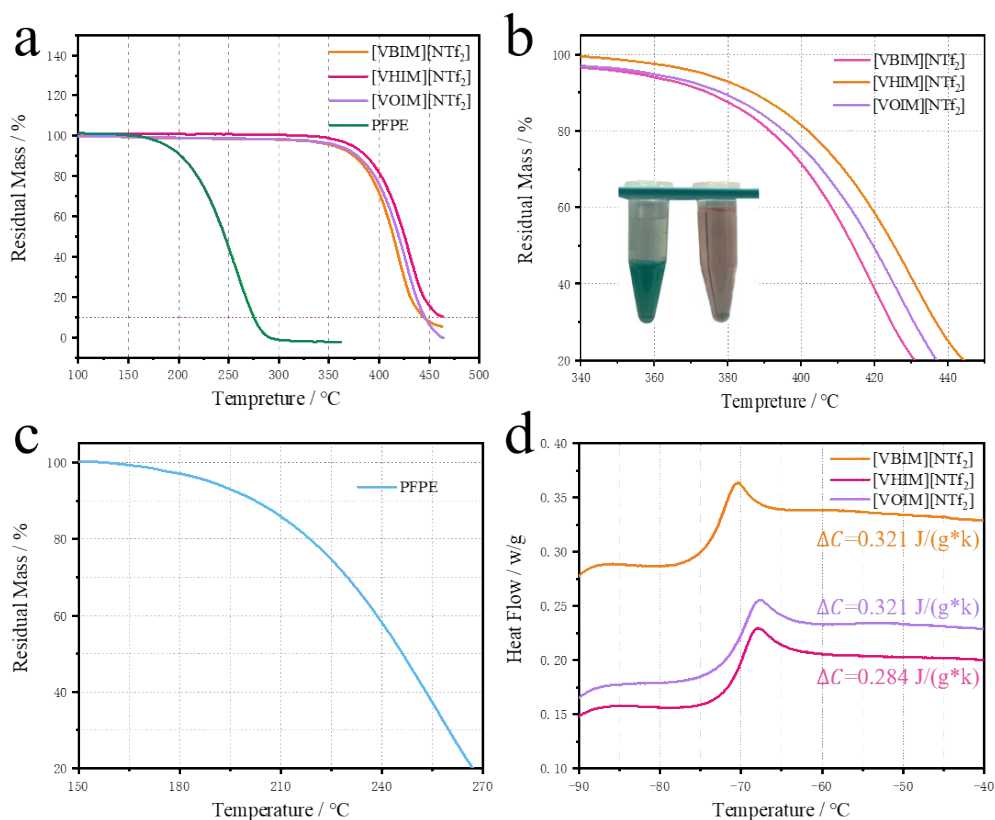
Fig. S1 TG curves of [VBIM][NTf$_2$], [VHIM][NTf$_2$], [VOIM][NTf$_2$] and PFPE (a), the initial decomposition curves of ILs (b) and PFPE (c), the inset image in the (b) is the optical images of the miscibility tests of [VHIM][NTf$_2$] with water dyed by MB (left) and ethanol dyed by RhB (right) after reaching a stable state, the DSC curves of ILs in the temperature-rise process (d).

Table S1 The T_d, $T_{10\%}$ and T_g of ILs and PFPE.

Lubricants	[VBIM][NTf$_2$]	[VHIM][NTf$_2$]	[VOIM][NTf$_2$]	PFPE
T_d (°C)	390.3	396.1	393.1	213.6
$T_{10\%}$ (°C)	443.8	463.3	445.6	274.6
T_g (°C)	-74.7	-71.8	-72.4	-78.8

2 The wettability of [VHIM][NTf$_2$]

Fig. S2 The wettability of [VHIM][NTf$_2$] on SC treated AAO surface with CA of 18.57 ± 0.42 °.

3 The relationship between pore size and capillarity

The Laplace equation (Eq1) can be expressed as the relationship between pore size and

capillarity.

$$\Delta P = \frac{2\gamma}{R}$$ (Eq1)

where ΔP, γ and R_1 represent the capillary pressure, surface tension of a liquid and curvature radius of the meniscus, respectively. Fig. S3 show the sketch map of a liquid wetting a pore, R, r and θ represent the curvature radius of the meniscus, radius of pore and the contact angle of a liquid on the contact surface, respectively. And there is relationship as $R = \frac{r}{\cos \theta}$. Based on that, the capillary pressure can be described as Eq2.

$$\Delta P = \frac{2\gamma \cos \theta}{r}$$ (Eq2)

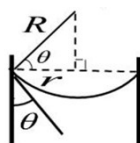Fig. S3 The sketch map of a liquid with surface tension of γ wetting a pore with radius of r.

As discussed above, the capillary pressure is inversely proportional to the radius of pores, indicating that the larger the radius of pores, the smaller the capillary pressure. Therefore, the PIL/AAO with thinner pores has larger capillary pressure than that of AAO with thicker pores. That also means the PIL/AAO surface with pore size of about 100 nm had stronger capillarity.

4 The density of [VHIM][NTf$_2$]

The density of [VHIM][NTf$_2$] was tested by capillary stoppered pycnometer method. The temperature of tested liquid should lower than the test temperature according to the contraction principle, and water was employed as standard liquid. The pycnometer filled with water was maintained at 20 $^\circ$C for 30 min to ensure water fill the pycnometer completely and there wasn't excess water overflow. The pycnometer filled with [VHIM][NTf$_2$] was maintained at 20 $^\circ$C for 30 min, too. According to the GB/T-13377, the density was calculated by means of calculation equation (Eq3):

$$\rho_t = \frac{m_t - m_o}{m_c - m_0}\rho_c + C$$ (Eq3)

where the ρ_t, ρ_c, m_o, m_c, m_t and C represent the density of [VHIM][NTf$_2$] and water at 20 $^\circ$C, the mass of empty pycnometer, pycnometer filled with water, pycnometer filled with [VHIM][NTf$_2$] and the air buoyancy correction index, respectively. The m_o, m_c and m_t were 11.7791, 16.5302 and 18.2852g, respectively. ρ_c and C were 998.2057 g/mL and -0.0024°C^{-1} at 20 $^\circ$C, respectively. Based on that, the ρ_t was 1.364 g/mL at 20 $^\circ$C.

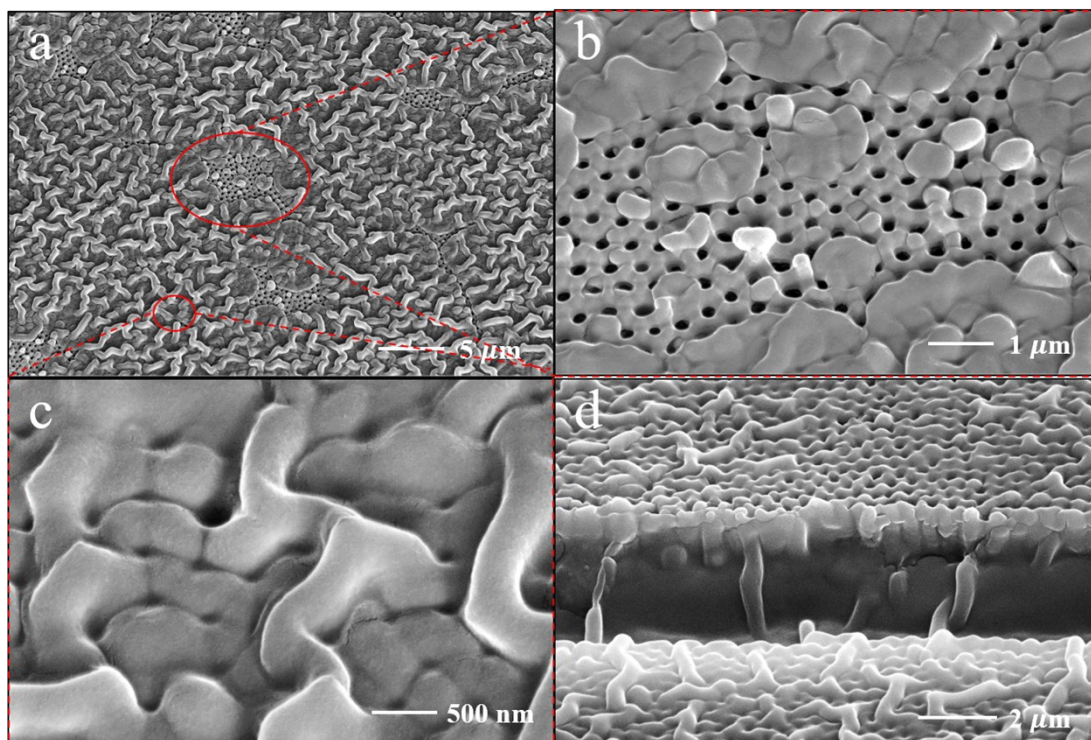**5 The surface morphology of lacking the pretreatment steps**

Fig. S4 SEM images of PIL inadequacy tiled on the AAO surfaces due to the lack of the pretreatment steps. The overall view of the excessive polymerization state (a), the inadequacy (b) and adequacy (c) covered porous, the profile of PIL inadequacy tiled surfaces the profile of PIL/AAO surfaces (g-i) with reserved pores.

6 The temperature stability of SLIPSs

Table S2 The CA and SA of different samples.

Samples	AAO	IL/AAO	PIL/AAO	IL/PIL/AAO
CA ($^\circ$)	91.10 $\pm$ 0.98	63.97 $\pm$ 0.57	87.33 $\pm$ 0.25	62.43 $\pm$ 0.51
SA ($^\circ$)	>90	2.54 $\pm$ 0.13	>90	1.35 $\pm$ 0.09

Table S3 The CA and SA of underwater stability tests for IL/PIL/AAO.

Time (h)	1	2	3	4	5
CA ($^\circ$)	56.00 $\pm$ 0.26	57.80 $\pm$ 0.10	55.20 $\pm$ 0.35	58.57 $\pm$ 0.60	57.37 $\pm$ 0.35
SA ($^\circ$)	1.49 $\pm$ 0.05	1.41 $\pm$ 0.04	1.39 $\pm$ 0.04	1.23 $\pm$ 0.03	2.38 $\pm$ 0.01
Time (h)	6	7	8	9	10
CA ($^\circ$)	60.27 $\pm$ 0.06	62.93 $\pm$ 0.15	63.13 $\pm$ 0.15	62.60 $\pm$ 0.35	63.70 $\pm$ 0.20
SA ($^\circ$)	1.85 $\pm$ 0.05	2.11 $\pm$ 0.04	2.05 $\pm$ 0.05	3.07 $\pm$ 0.12	3.26 $\pm$ 0.02

Table S4 The CA and SA at gradient temperature tests of IL/PIL/AAO.

Temperature (°C)	-20	0	60	80	100
CA (°)	55.2 ± 0.87	56.33 ± 0.35	55.10 ± 0.36	55.00 ± 0.44	58.00 ± 0.10
SA (°)	1.22 ± 0.06	1.21 ± 0.01	1.38 ± 0.07	1.68 ± 0.12	1.90 ± 0.13
Temperature (°C)	120	150	180	200	220
CA (°)	61.63 ± 0.45	61.87 ± 0.47	63.93 ± 0.81	64.30 ± 0.45	66.10 ± 0.36
SA (°)	1.91 ± 0.02	1.97 ± 0.06	2.63 ± 0.05	2.82 ± 0.02	3.48 ± 0.06

Table S5 The CA and SA during the temperature stability.

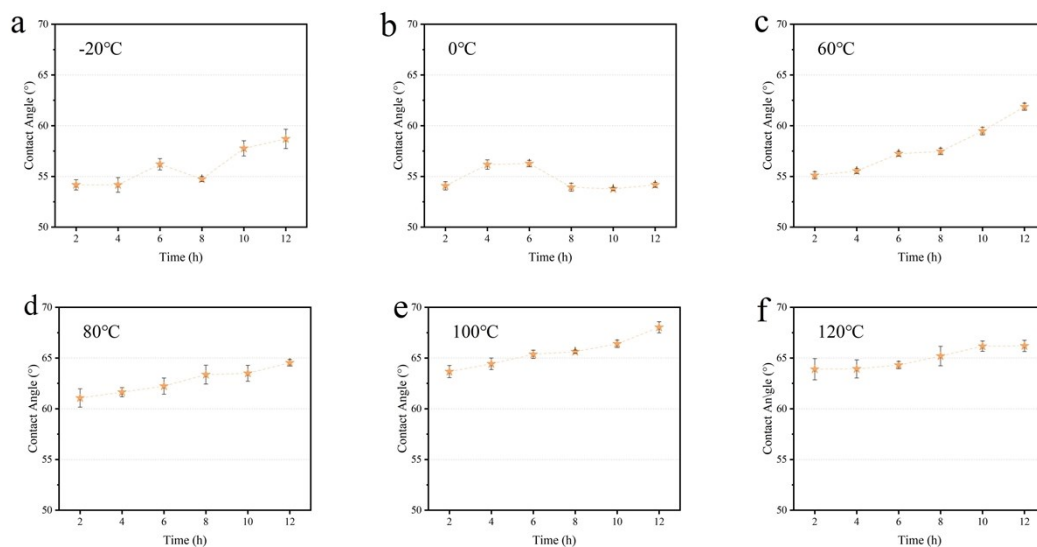| Temperature (°C)	-20	0	60	80	100	120
$\overline{CA}$ (°)	55.96 ± 1.94	54.73 ± 1.16	57.90 ± 4.24	62.72 ± 1.30	65.51 ± 2.15	64.95 ± 1.06
$\overline{SA}$ (°)	1.40 ± 0.13	1.11 ± 0.28	1.75 ± 0.34	1.60 ± 0.48	2.12 ± 0.55	2.66 ± 0.54

Fig. S5 The CA vibration of IL/PIL/AAO at -20 (a), 0 (b), 60 (c), 80 (d), 100 (e) and 120 °C (f) within 12 h.
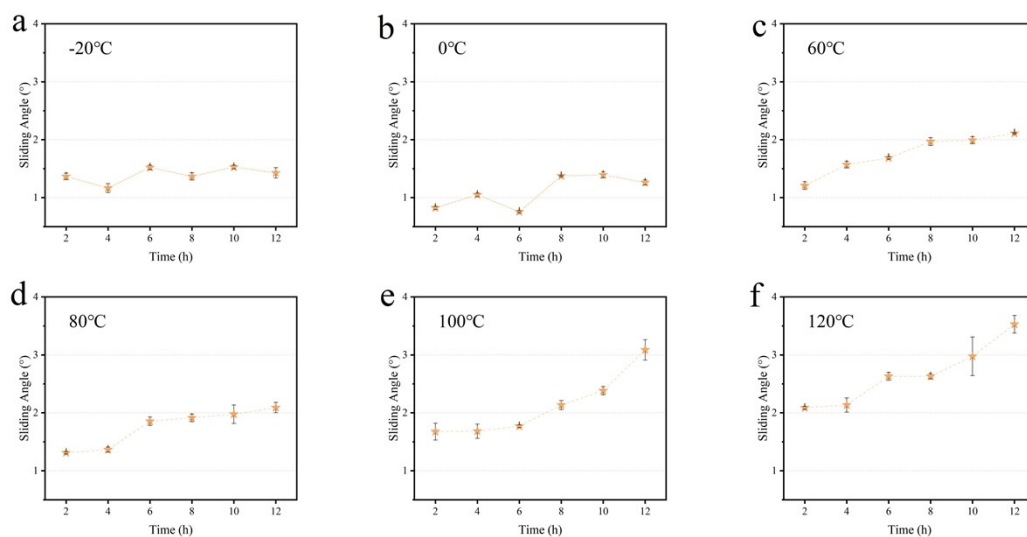
Fig. S6 The SA vibration of IL/PIL/AAO at -20 (a), 0 (b), 60 (c), 80 (d), 100 (e) and 120 °C (f) within 12 h.
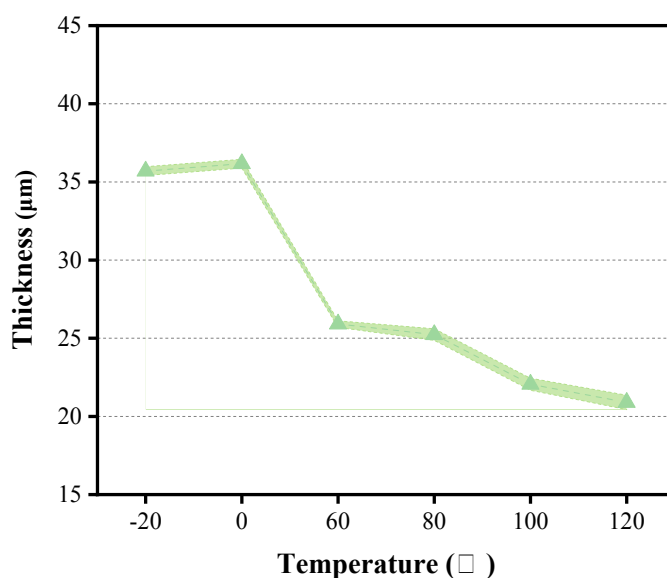

Fig. S7 The ILs thickness after maintain at -20, 0, 60, 80, 100 and 120 °C for 12 h of IL/PIL/AAO.

Table S6 The ILs thickness after maintain at -20, 0, 60, 80, 100 and 120 °C for 12 h of IL/PIL/AAO.

Temperature (°C)	-20	0	60	80	100	120
Thickness (μm)	35.68 ± 0.28	36.17 ± 0.28	25.91 ± 0.21	25.23 ± 0.37	22.06 ± 0.38	20.90 ± 0.46

The IL thickness on PIL/AAO surface was calculated based on the relationship between the remaining ILs content and volume. The pore volume of AAO and PIL/AAO surfaces were calculated based on the pore size, pore depth and pore distance, and were about $620 \times 10^{-7}\ cm^3$ and

$223 \times 10^{-7}\ cm^3$, respectively, which was negligible to the volume of ILs on the surface.

7 The shear resistance of SLIPSs

Table S7 The ILs content per unit area, CA and SA of IL/AAO surface within spin rate of 1000-7000 rpm.

Spin Rate (rpm)	1000	2000	3000	4000	5000	6000	7000
ILs Content (mg/cm^{-2})	3.37 ± 0.01	1.58 ± 0.05	0.99 ± 0.04	0.75 ± 0.03	0.54 ± 0.04	0.45	0.37 ± 0.04
CA (°)	54.87 ± 0.32	63.97 ± 0.57	65.33 ± 0.31	66.87 ± 0.32	66.93 ± 0.47	67.47 ± 0.23	68.7 ± 0.53
SA (°)	1.05 ± 0.05	2.54 ± 0.13	3.82 ± 0.15	3.87 ± 0.05	3.60 ± 0.17	4.29 ± 0.07	6.69 ± 0.08

Table S8 The ILs content per unit area, CA and SA of IL/PIL/AAO surface within spin rate of 1000-7000 rpm.

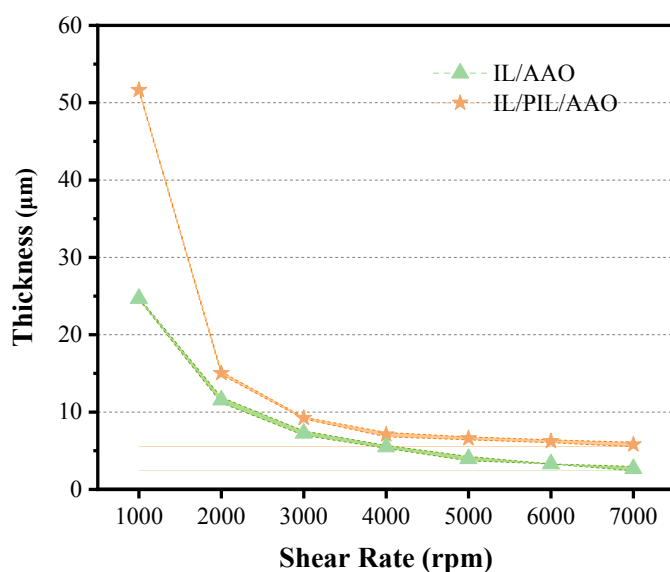| Spin Rate (rpm)	1000	2000	3000	4000	5000	6000	7000
ILs Content (mg/cm^{-2})	7.04 ± 0.01	2.05 ± 0.03	1.26 ± 0.01	0.97 ± 0.04	0.90 ± 0.03	0.85 ± 0.03	0.79 ± 0.04
CA (°)	54.4 ± 0.2	62.43 ± 0.51	64.6 ± 0.1	64.93 ± 0.12	64.93 ± 0.95	66.4 ± 0.17	67.73 ± 0.15
SA (°)	0.73 ± 0.08	1.35 ± 0.09	1.61 ± 0.09	1.48 ± 0.17	1.48 ± 0.07	1.93 ± 0.11	2.29 ± 0.17

Fig. S8 The ILs thickness after suffer from shear force at spin rate of 1000-7000 rpm of IL/PIL/AAO and IL/PIL/AAO.

Table S9 The ILs thickness after suffer from shear force at spin rate of 1000-7000 rpm of

Spin Rate (rpm)	1000	2000	3000	4000	5000	6000	7000
Thickness of IL/ AAO (μm)	24.68 ± 0.11	11.55 ± 0.37	7.27 ± 0.28	5.50 ± 0.18	2.97 ± 0.28	3.30	2.68 ± 0.28
Thickness of IL/PIL/AAO (μm)	51.63 ± 0.11	15.03 ± 0.18	9.23 ± 0.11	7.09 ± 0.28	6.60 ± 0.18	6.23 ± 0.18	5.80 ± 0.28

IL/PIL/AAO and IL/PIL/AAO.

8 The corrosion resistance of SLIPSs

The inhibition efficiency (IE) was calculated from the following equation:

$$IE = \frac{I_{corr,\ AAO} - I_{corr,\ coted\ AAO}}{I_{corr,\ AAO}} \times 100\%$$

(Eq4)

Where the $I_{corr,\ AAO}$, $I_{corr,\ coted\ AAO}$ corresponding to the corrosion current density of untreated AAO and undergone surface-treated AAO, respectively[1].

Table S10 The E_{corr} and I_{corr} of different samples calculated by the Tafel curves.

	AAO	PIL/AAO	IL/PIL/AAO	AAO-B	PIL/AAO-B	IL/PIL/AAO-B
E_{corr} (v)	-0.764	-0.742	-0.701	-0.777	-0.718	-0.712
lg I_{corr}	-6.897	-8.011	-8.710	-6.448	-7.263	-8.108

(J, A cm^{-2})

9 The dye absorption of SLIPSs

The dye absorption efficiency was calculated by following equation:

$$E = \frac{A - A_x}{A} \times 100\%$$

(Eq5)

where A and A_x corresponding to the maximum absorbance before and after the $x\ ml$ absorption of dye, respectively[2].
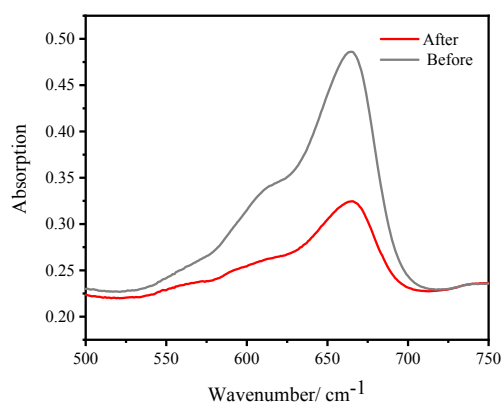

Fig. S9 The UV-vis spectra of 1.5 mg/L MB before and after slipping through the SLIPSs with a SA of 1.5 °.

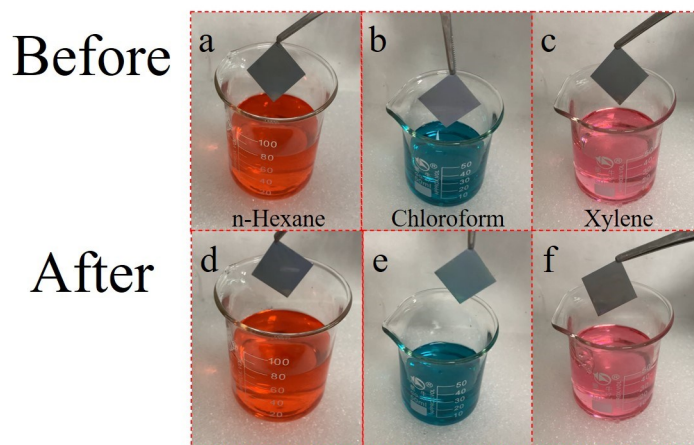**10 The dye absorption of SLIPSs**

Fig. S10 A series of resistance to organic solution contamination tests of the SLIPSs. The optical images of the SLIPSs before and after soaking in n-hexane (a, d), chloroform (b, e) and xylene (c, f).

The SLIPSs with resistance to organic solutions contamination are of great significance for extending the practical application of materials. The SLIPSs fabricated in this work exhibited excellent resistance to the nonpolar organic solutions, such as n-hexane, chloroform, xylene and so on. The n-hexane and xylene were dyed by Sudan III, and the chloroform was dyed by malachite green. As shown in Fig. S10, after it was soaked in the organic solutions, the original surfaces were as clean as it was at its beginning, which was attributed to the immiscibility of the [VHIM][NTf$_2$] to the nonpolar organic solutions. For the polar organic solutions, such as ethanol, acetonitrile,

formamide and so on, the SLIPSs had a weak resist due to the miscibility of the [VHIM][NTf$_2$].

11 References

1.   J. Lee, S. Shin, Y. Jiang, C. Jeong, H. A. Stone and C.-H. Choi, *Adv. Funct. Mater.*, 2017, **27**.
2.   Y. Sun, M. Liu and Z. Guo, *J. Colloid Interface Sci.*, 2018, **527**, 187-194.

Movie S1. The slippery behaviors of 10 μL drop on the SLIPSs before and after heavy scratches.

Movie S2. The slippery behavior of the SLIPSs at 220 $^{\circ}$C.

Movie S3. The slippery behaviors of different re-infused cycles of the SLIPSs at 7000 rpm.